

A new oscillatory instability in a mushy layer during the solidification of binary alloys

By D. M. ANDERSON† AND M. GRAE WORSTER

Institute of Theoretical Geophysics, Department of Applied Mathematics and Theoretical Physics,
University of Cambridge, Silver Street, Cambridge CB3 9EW, UK

(Received 5 July 1995)

We consider the solidification of a binary alloy in a mushy layer and analyse the linear stability of a quiescent state with specific interest in identifying an oscillatory convective instability. We employ a near-eutectic approximation and consider the limit of large far-field temperature. These asymptotic limits allow us to examine the dynamics of the mushy layer in the form of small deviations from the classical case of convection in a horizontal porous layer of uniform permeability. We consider also the limit of large Stefan number, which incorporates a key balance necessary for the existence of the oscillatory instability. The model we consider here contains no double-diffusive effects and no region in which a statically stable density gradient exists. The mechanism underlying the oscillatory instability we discover is instead associated with a complex interaction between heat transfer, convection and solidification.

1. Introduction

When a binary mixture solidifies from a cold boundary, the planar solidification front often becomes unstable due to constitutional undercooling (see Kurz & Fisher 1989). The result is a mushy layer, separating the completely liquid phase from the completely solid phase. The mushy layer is a reactive porous medium, whose internal structure is composed of fine-scale crystals, through which the residual melt can flow.

Compositional convection can occur in a mushy layer cooled from below when unstable density gradients are formed as a result of rejection of the lighter component of the mixture upon solidification. The dynamic response of the mushy layer is driven by the interaction between convection, heat transfer and solidification. The convective transport of heat and solute can alter the solid matrix of the mushy layer, which in turn modifies the flow. A dramatic example of this is the formation of chimneys in the mushy layer. Chimneys are localized channels devoid of solid through which buoyant liquid rises, as observed experimentally by a number of investigators (e.g. Copley *et al.* 1970; Sample & Hellawell 1984; Sarazin & Hellawell 1988; Chen & Chen 1991; Tait & Jaupart 1992; Tait, Jahrling & Jaupart 1992).

The observations of chimneys in mushy layers have led to theoretical investigations that have focused on a direct mode of instability. Fowler (1985) proposed a model for a mushy layer and analysed a limiting case in which the mushy layer behaves as a non-reacting porous layer. Worster (1992*b*) analysed the linear stability of convection in a mushy layer in which he included the effects of the interaction of convection

† Present address: Applied and Computational Mathematics Division, National Institute of Standards and Technology, Gaithersburg, MD 20899, USA.

and solidification in the mushy layer. He identified two direct modes of convective instability: one driven from a narrow compositional boundary layer above the mush-liquid interface and the other driven from the interior of the mushy layer. Emms & Fowler (1994) performed a linear stability analysis which involved a time-dependent basic state. In contrast to Worster's (1992*b*) analysis which determined stability relative to a motionless basic state, the linear stability of the mushy-layer convection was determined relative to a basic state that included the effects of double-diffusive, finger-type convection in the liquid. However, the influence of the convection in the liquid region upon the mushy layer was found to be negligible in their analysis, indicating that the onset of convection in the mushy layer is little affected by vigorous convection in the melt.

Recently, Chen, Lu & Yang (1994) extended Worster's (1992*b*) stability analysis of convection in the mushy layer and found that, when stabilizing thermal buoyancy is present in the liquid, the two steady modes of convection can separate by way of an oscillatory instability. This was the first theoretical analysis of the mushy layer to consider and identify oscillatory modes. They analysed the properties of this oscillatory branch of solutions and determined its behaviour as parameters such as the compositional ratio, far-field temperature, Darcy number, Lewis number and Prandtl number were varied. In all of the cases in which the oscillatory instability was present, the buoyancy ratio (thermal to solutal) in the liquid region was nonzero. When the buoyancy ratio was taken to be zero, this oscillatory instability ceased to exist. Accordingly, they associated this oscillatory instability with the interaction of the double-diffusive convection in the liquid region with the mushy-layer convective mode. In their results the steady modes always became unstable before the oscillatory mode.

Nonlinear stability analyses of convection in mushy layers have to date been applied only to steady modes of instability. Amberg & Homsy (1993) performed a weakly nonlinear analysis of convection in a mushy layer using a model in which the mushy layer is decoupled from the overlying liquid layer and the underlying solid layer. Their analysis revealed the structure of possible nonlinear, steady convecting states in the mushy layer. Anderson & Worster (1995) extended the analysis of Amberg & Homsy and determined the stability of nonlinear solutions that included additional physical effects and interactions in the mushy layer. The pivotal result of their analysis was a set of amplitude equations which described the evolution of small-amplitude convecting states associated with direct modes of instability. They interpreted these equations in terms of stability and pattern-selection criteria. Additionally, however, inspection of their amplitude equations indicated the possibility of an oscillatory mode of instability despite the lack of any stabilizing thermal buoyancy, in contrast with the results of Chen *et al.* (1994). Their analysis of the nonlinear development of the steady mode of convection was therefore restricted to parameter regimes in which the oscillatory instability did not interact with the steady mode near onset. It is the nature of this oscillatory instability which we shall elucidate here.

In the present paper, we investigate the mushy-layer model of Amberg & Homsy (1993) using a linear stability analysis to identify and describe the oscillatory instability whose existence was suggested by the analysis of Anderson & Worster (1995). It is important to note at the outset that, since no region of static stability is present in this model, the oscillatory mode described here is necessarily distinct from that found by Chen *et al.* (1994). We shall find that owing to the nature of the present mushy-layer model, which isolates the mushy layer from the rest of the system, the oscillations

are a consequence of an internal mechanism associated with a complex interaction between heat transfer, convection and solidification in the mushy layer.

The paper is structured as follows. In §2 we describe the model. In §3 we perform a linear stability analysis and derive the associated characteristic equation which relates the linear growth rate with the wavenumber of the perturbation. In §4 we analyse the characteristic equation and identify and describe the modes of instability present. In §5 we address the physical mechanisms associated with the oscillatory instability. Finally, in §6 we give the conclusions.

2. Formulation

The model we analyse is that given in Amberg & Homay (1993) and later used by Anderson & Worster (1995). For clarity, we describe the key aspects of the model here.

The physical system we are interested in is one in which a binary alloy is cooled from below and solidifies releasing a buoyant residual. For mathematical ease we consider a system solidifying at a prescribed constant speed V . This would be the case during the directional casting of turbine blades, for example. In this case, a mushy layer is sandwiched between a completely solid region below (at temperatures below the eutectic) and a completely liquid region above, as shown in figure 1. The liquid far above the mushy layer has a composition $C_0 > C_E$ and temperature $T_\infty > T_L(C_0)$ where C_E is the eutectic composition and $T_L(C)$ is the liquidus temperature of the alloy. The model is simplified (Amberg & Homay 1993) by assuming that the mushy layer is physically isolated, and hence dynamically decoupled, from the overlying liquid and underlying solid regions. This is accomplished by requiring that the mushy layer have rigid and isothermal upper and lower boundaries at which the vertical component of the fluid velocity is zero. We fix our coordinates in a frame of reference moving with the mushy layer at the solidification speed V . The mushy layer is also assumed to have constant thickness d . These are simplifying assumptions which make the problem analytically tractable but which do not take away the essential physics internal to the mushy layer associated with interactions between heat transfer, convection and solidification.

The mushy layer is assumed to be in local thermodynamic equilibrium so that the temperature T is related to the composition C via the linear liquidus relation

$$T = T_L(C_0) + \Gamma(C - C_0), \quad (2.1)$$

where Γ is the slope of the liquidus. As a result of this direct coupling between temperature and composition, there are no double-diffusive effects within the mushy layer. This immediately rules out double-diffusion as a mechanism for oscillatory instability in the mushy layer. The liquid density is linearly related to the temperature and composition and from equation (2.1) can be written as

$$\rho_l = \rho_0[1 + \beta(C - C_0)], \quad (2.2)$$

where $\beta = \beta^* - \Gamma\alpha^*$ and α^* and β^* are the thermal and compositional expansion coefficients, respectively. Note that typically $\beta^* > \Gamma\alpha^*$, so that β is positive.

We have used the following scalings to render the governing equations dimensionless. The velocity scale is V , the length and time scales are given by the thermal diffusion length and time, κ/V and κ/V^2 , where κ is the thermal diffusivity of the liquid. The pressure scale is $\kappa\mu/\Pi(0)$ where μ is the dynamic viscosity of the liquid and $\Pi(0)$ is a measure of the permeability of the mushy layer as described below

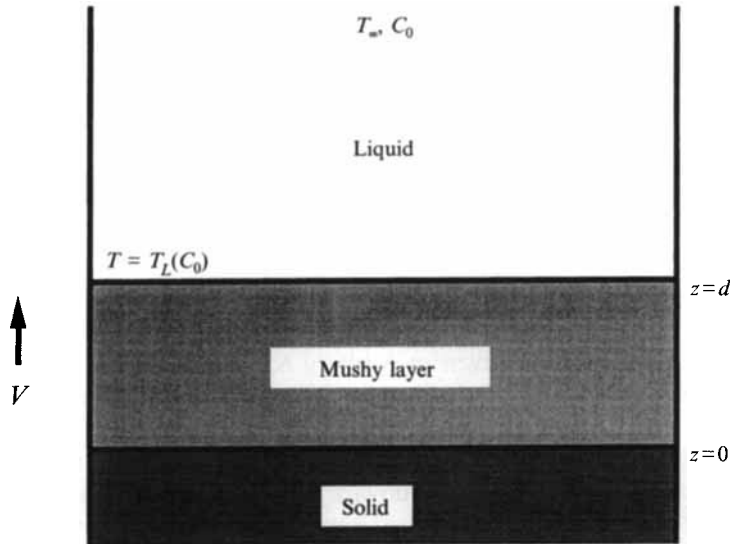


FIGURE 1. The mushy-layer system. A binary alloy is cooled from below and releases a buoyant residual upon solidification. The mushy layer is sandwiched between a solid layer (of temperature below the eutectic temperature T_E) and a liquid layer (of temperature above the liquidus temperature $T_L(C_0)$). The liquid far above the mushy layer has a composition C_0 and a temperature $T_\infty > T_L(C_0)$. The mushy layer is assumed to grow upwards into the liquid at a constant speed V and is assumed to have constant thickness d . The mushy layer is taken to have rigid and isothermal upper and lower boundaries at which the vertical component of the fluid velocity is zero. Note that composition at the mush-liquid interface is C_0 while that at the mush-solid interface is C_E and that, owing to the advancement of the mushy layer, there are solute fluxes both into and out of the mushy layer. These are simplifying steps which effectively decouple the dynamics of the mushy layer from the rest of the system.

in equation (2.6). The nondimensional temperature (or equivalently composition) is given by

$$\theta = \frac{T - T_L(C_0)}{\Delta T} = \frac{C - C_0}{\Delta C}, \quad (2.3)$$

where $\Delta T = T_L(C_0) - T_E$ and $\Delta C = C_0 - C_E$ so $\Delta T = \Gamma \Delta C$.

The nondimensional equations governing the mushy layer in a reference frame moving at speed V are the heat balance, solute balance, Darcy's equation, and mass balance given by

$$\left(\frac{\partial}{\partial t} - \frac{\partial}{\partial z} \right) (\theta - S\phi) + \mathbf{u} \cdot \nabla \theta = \nabla^2 \theta, \quad (2.4a)$$

$$\left(\frac{\partial}{\partial t} - \frac{\partial}{\partial z} \right) ((1 - \phi)\theta + \mathcal{C}\phi) + \mathbf{u} \cdot \nabla \theta = 0, \quad (2.4b)$$

$$K(\phi)\mathbf{u} = -\nabla p - Ra\theta\hat{z}, \quad (2.4c)$$

$$\nabla \cdot \mathbf{u} = 0. \quad (2.4d)$$

The basis for these equations rests on the idea that, owing to its fine-scale structure, the mushy layer can be treated as a continuum. The derivation and justification of such equations as continuum descriptions of the mushy layer have been put forward by a number of previous authors (e.g. Hills, Loper & Roberts 1983; Worster 1986; Bennon & Incropera 1987; Voller & Brent 1989; Worster 1992a). The present formulation

and notation is most similar to Worster (1992*b*), which was also used by Amberg & Homsy (1993) and Anderson & Worster (1995). We have taken the material properties of the solid and liquid phases to be equal and have neglected diffusion of solute. Note, however, that since the mushy layer is in thermodynamic equilibrium, retaining the effect of solute diffusion here would only modify the coefficient of the diffusion term in equation (2.4*a*) but slightly. The dimensionless parameters appearing in these equations are the Stefan number S , the concentration ratio \mathcal{C} , and the Rayleigh number Ra , where

$$S = \frac{L}{c_l \Delta T}, \tag{2.5a}$$

$$\mathcal{C} = \frac{C'_S - C_0}{C_0 - C_E}, \tag{2.5b}$$

$$Ra = \frac{\beta \Delta C g \Pi(0) \kappa / V}{\nu \kappa}, \tag{2.5c}$$

where L is the latent heat, c_l is the specific heat, C'_S is the solid composition, C_E is the eutectic composition, g is acceleration due to gravity, and ν is the kinematic viscosity of the liquid. The Stefan number S represents a measure of the latent heat relative to the heat content, or available heat in the system. The compositional ratio \mathcal{C} relates the difference in characteristic compositions of the liquid and solid phases to the compositional variation across the mushy layer. Large values of \mathcal{C} , which we shall consider shortly, correspond to initial compositions that are near the eutectic composition. The Rayleigh number Ra measures the destabilizing influence of compositional buoyancy relative to the stabilizing influences of thermal diffusion and viscous drag.

The function $K(\phi)$ measures the variation of the permeability $\Pi(\phi)$ with local solid fraction ϕ and is given by

$$K(\phi) = \frac{\Pi(0)}{\Pi(\phi)}, \tag{2.6}$$

where the permeability is assumed to be finite for zero solid fraction. Such an assumption, as discussed by Worster (1992*b*), is appropriate when Darcy's equation, rather than a more general Brinkman equation, which includes the effects of inertia and deviatoric stresses in the mushy layer, is used to describe the flow.

Equations (2.4) are subject to the boundary conditions

$$\theta = -1, \quad w = 0 \quad \text{at} \quad z = 0, \tag{2.7a,b}$$

$$\theta = 0, \quad w = 0, \quad \phi = 0 \quad \text{at} \quad z = \delta, \tag{2.8a-c}$$

where $\delta = d/(\kappa/V)$ is the dimensionless depth of the layer. On the solid–mush interface $z = 0$ the temperature is the eutectic temperature and the vertical component of the fluid velocity is zero. On the mush–liquid interface $z = \delta$ the temperature is the liquidus temperature, the vertical component of the fluid velocity is zero, and the solid fraction is zero. Note that the mush–liquid interface corresponds to composition C_0 and the mush–solid interface corresponds to composition C_E . Owing to the advancement of the mushy layer, there are solute fluxes both into and out of the mushy layer.

The hydrodynamic boundary condition for the two-layer problem in which the mushy layer and liquid layer are dynamically coupled is one of continuity of pressure $[p] = 0$ at the mush–liquid interface. This condition reduces to that of $p = \text{constant}$

on the mush–liquid interface in the limit of zero Darcy number $Da = \Pi(0)/(\kappa/V)^2$, where the Darcy number measures the ratio of the average spacing between the dendrites in the mushy layer to the thermal length (Emms & Fowler 1994). Here we are imposing artificially the no-flow condition (2.8b) instead of the pressure condition and we are additionally keeping the position of the interface $z = \delta$ fixed. In the full system, if the stabilizing buoyancy in the liquid region is large, the streamlines from the mushy layer do not penetrate far into the liquid region and the upper boundary of the mushy layer behaves like a rigid lid, as we have imposed here. It can be anticipated that the no-flow boundary condition will act to inhibit the motion of the fluid in the mushy layer by not allowing it to convect freely into the upper liquid layer. The results of Chen *et al.* (1994) have in fact shown that when stabilizing buoyancy in the liquid region is large the critical Rayleigh number is approximately twice that for the system with a constant-pressure boundary. The boundary conditions imposed at the mush–liquid interface, with the exception of the no-flow condition and the assumption that the interface is non-deformable, can be derived in the asymptotic limit of large Lewis number (ratio of thermal to solutal diffusivities) from the boundary conditions used in the full model (see Emms & Fowler 1994). Anderson & Worster (1995) discussed further the merits of these boundary conditions and argued that while they greatly simplify the analysis, they do not compromise the essence of the interactions between heat flow, convection and solidification in the mushy layer.

We follow Anderson & Worster (1995) in reducing the model asymptotically. We assume that the mushy layer is thin so $\delta \ll 1$. The dimensionless mushy layer thickness can be associated with the inverse of the non-dimensional far-field temperature $\theta_\infty = T_\infty/\Delta T$ for $\theta_\infty \gg 1$ (e.g. see Fowler 1985; Worster 1991). We also consider the limit where \mathcal{C} is large. Physically, this occurs when the initial composition of the liquid is close to the eutectic composition as can be seen by the definition of \mathcal{C} in equation (2.5b). Specifically, we take

$$\mathcal{C} = \frac{C_S}{\delta}, \quad (2.9)$$

where C_S is $O(1)$ as $\delta \rightarrow 0$. The above approximation ($\delta \rightarrow 0$, $\mathcal{C} \rightarrow \infty$) corresponds to the near-eutectic approximation used by Fowler (1985). This limit allows for the leading-order description of the mushy layer as a porous layer of constant permeability. The idea is then to re-introduce effects such as permeability variations as perturbations to this simpler system. In contrast to Amberg & Homsy (1993) who kept $S = O(1)$, we follow Emms & Fowler (1994) and Anderson & Worster (1995) and assume that the Stefan number is large by writing

$$S = \frac{\bar{S}}{\delta}, \quad (2.10)$$

where \bar{S} is $O(1)$ as $\delta \rightarrow 0$. We shall find that this is a key step which allows us to identify a new oscillatory instability from our analysis. We rescale space and time and also introduce a new effective Rayleigh number R based on the mushy-layer thickness δ :

$$(x, z) = \delta(\bar{x}, \bar{z}), \quad t = \delta^2 \bar{t}, \quad R^2 = \delta Ra. \quad (2.11a-c)$$

The timescale represented here is associated with the diffusion time across the layer. Finally, we introduce the following rescalings as used in the nonlinear analyses of

Amberg & Homsy (1993) and Anderson & Worster (1995):

$$\mathbf{u} = \frac{R}{\delta} \bar{\mathbf{u}}, \quad p = R\bar{p}. \quad (2.12a,b)$$

There is a steady basic state, denoted by subscript 'B', which is horizontally uniform, corresponds to zero flow and satisfies

$$-\delta \frac{d}{d\bar{z}} \left[\theta_B - \frac{\bar{S}}{\delta} \phi_B \right] = \frac{d^2 \theta_B}{d\bar{z}^2}, \quad (2.13a)$$

$$-\delta \frac{d}{d\bar{z}} \left[(1 - \phi_B) \theta_B + \frac{C_S}{\delta} \phi_B \right] = 0, \quad (2.13b)$$

$$-\frac{dp_B}{d\bar{z}} - R\theta_B = 0, \quad (2.13c)$$

subject to the boundary conditions

$$\theta_B = -1 \quad \text{at} \quad \bar{z} = 0, \quad (2.14)$$

$$\theta_B = 0, \quad \phi_B = 0 \quad \text{at} \quad \bar{z} = 1. \quad (2.15a,b)$$

We can express the basic-state solutions in terms of asymptotic expansions for $\delta \ll 1$:

$$\theta_B = (\bar{z} - 1) - \delta \frac{\Omega}{2} (\bar{z}^2 - \bar{z}) + \dots, \quad (2.16a)$$

$$\phi_B = \delta \bar{\phi}_B = -\delta \frac{\bar{z} - 1}{C_S} + \delta^2 \left(-\frac{(\bar{z} - 1)^2}{C_S^2} + \frac{\Omega}{2C_S} (\bar{z}^2 - \bar{z}) \right) + \dots, \quad (2.16b)$$

where $\Omega = 1 + \bar{S}/C_S = 1 + S/\mathcal{C}$. Note that the assumption $\mathcal{C} \sim O(1/\delta)$ leads to a small basic-state solid fraction of $O(\delta)$.

3. Linear stability analysis

We introduce normal-mode perturbations to the basic-state solution as follows:

$$\theta = \theta_B + \hat{\theta}(\bar{z}) e^{\sigma t} e^{ik\bar{x}} + \text{c.c.}, \quad (3.1a)$$

$$\phi = \phi_B + \hat{\phi}(\bar{z}) e^{\sigma t} e^{ik\bar{x}} + \text{c.c.}, \quad (3.1b)$$

$$\bar{\mathbf{u}} = \mathbf{0} + \hat{\mathbf{u}}(\bar{z}) e^{\sigma t} e^{ik\bar{x}} + \text{c.c.}, \quad (3.1c)$$

where σ is the growth rate and k is the horizontal wavenumber of the perturbation. We express the growth rate $\sigma = \sigma_R + i\sigma_I$ in terms of real and imaginary parts, insert the normal-mode forms into the governing equations (2.4), linearize, and find that the perturbation quantities satisfy

$$(\sigma_R + i\sigma_I - \delta D) \left(\hat{\theta} - \frac{\bar{S}}{\delta} \hat{\phi} \right) + R\hat{w}D\theta_B = -k^2 \hat{\theta} + D^2 \hat{\theta}, \quad (3.2a)$$

$$(\sigma_R + i\sigma_I - \delta D) \left((1 - \delta \bar{\phi}_B) \hat{\theta} - \theta_B \hat{\phi} + \frac{C_S}{\delta} \hat{\phi} \right) + R\hat{w}D\theta_B = 0, \quad (3.2b)$$

$$D^2 (K(\delta \bar{\phi}_B) \hat{w}) - k^2 K(\delta \bar{\phi}_B) \hat{w} - k^2 R \hat{\theta} = D [\hat{w} D (K(\delta \bar{\phi}_B))], \quad (3.2c)$$

$$D^2 (K(\delta \bar{\phi}_B) \hat{u}) - k^2 K(\delta \bar{\phi}_B) \hat{u} - ikRD\hat{\theta} = ik [\hat{w} D (K(\delta \bar{\phi}_B))], \quad (3.2d)$$

subject to the boundary conditions

$$\hat{\theta} = 0, \quad \hat{w} = 0 \quad \text{at} \quad \bar{z} = 0, \quad (3.3a,b)$$

$$\hat{\theta} = 0, \quad \hat{w} = 0, \quad \hat{\phi} = 0 \quad \text{at} \quad \bar{z} = 1, \quad (3.4a-c)$$

where $D \equiv d/d\bar{z}$. Note that, for this linear theory, it is sufficient to consider two-dimensional perturbations.

We are interested in the solution to these equations for $\delta \ll 1$ so we expand the variables in powers of δ . We take

$$\sigma_R = \sigma_{R0} + \delta\sigma_{R1} + \dots, \quad (3.5a)$$

$$\sigma_I = \sigma_{I0} + \delta\sigma_{I1} + \dots, \quad (3.5b)$$

$$R = R_0 + \delta R_1 + \dots, \quad (3.5c)$$

$$\hat{\theta} = \theta_0 + \delta\theta_1 + \dots, \quad (3.5d)$$

$$\hat{\phi} = \phi_0 + \delta\phi_1 + \dots, \quad (3.5e)$$

$$\hat{w} = w_0 + \delta w_1 + \dots, \quad (3.5f)$$

$$K(\delta\bar{\phi}_B) = 1 + \delta\phi_{B0}K_1 + \dots \quad (3.5g)$$

Note that since the basic-state solid fraction is small, the permeability function $K(\phi)$ is expanded in a Taylor series. From equation (2.16b) $\phi_{B0} = (1 - \bar{z})/C_S$. The constant coefficient K_1 characterizes the linear variation of the permeability with the local solid fraction and must be positive so that the permeability decreases with increasing solid fraction. Further, it is clear from (3.5g) that the leading-order permeability is constant. In the limit $\delta \rightarrow 0$ we find that the system corresponds to convection in a passive porous medium with a linear temperature gradient as considered by Palm, Weber & Kvernold (1972). Effects which are fundamental to the mushy layer are re-introduced as small perturbations, of order δ , to this simpler system.

We proceed by expanding equations (3.2) in powers of δ . We use the solute balance (3.2b) to substitute for the terms involving the solid fraction perturbation $\hat{\phi}$ in the heat balance (3.2a). Subsequently, we find that there is an $O(1/\delta)$ problem only from the solute balance

$$(\sigma_{R0} + i\sigma_{I0})C_S\phi_0 = 0. \quad (3.6)$$

This equation is solved by taking $\sigma_{R0} = \sigma_{I0} = 0$. Note that this result suggests an oscillatory timescale different than the $O(\delta^2)$ timescale indicated by the scaling in equation (2.11b).

At $O(\delta^0)$ we find that

$$D^2\theta_0 - k^2\theta_0 - \Omega R_0 w_0 = 0, \quad (3.7a)$$

$$C_S(\sigma_{R1} + i\sigma_{I1} - D)\phi_0 + R_0 w_0 = 0, \quad (3.7b)$$

$$D^2 w_0 - k^2 w_0 - R_0 k^2 \theta_0 = 0, \quad (3.7c)$$

$$D^2 u_0 - k^2 u_0 - ikR_0 D\theta_0 = 0, \quad (3.7d)$$

with boundary conditions $\theta_0(0) = \theta_0(1) = 0$, $w_0(0) = w_0(1) = 0$ and $\phi_0(1) = 0$, where $\Omega = 1 + \bar{S}/C_S$.

The solutions at this order are given by

$$\theta_0 = -\sin \pi \bar{z}, \quad (3.8a)$$

$$\phi_0 = -\frac{\pi(k^2 + \pi^2)}{\Omega C_S [\pi^2 + (\sigma_{R1} + i\sigma_{I1})^2]} \left[e^{(\sigma_{R1} + i\sigma_{I1})(\bar{z}-1)} + \cos \pi \bar{z} + \frac{\sigma_{R1} + i\sigma_{I1}}{\pi} \sin \pi \bar{z} \right], \quad (3.8b)$$

$$w_0 = \frac{k^2 + \pi^2}{\Omega R_0} \sin \pi \bar{z}, \quad (3.8c)$$

$$u_0 = ik \frac{\pi R_0}{k^2 + \pi^2} \cos \pi \bar{z}, \quad (3.8d)$$

$$R_0^2 = \frac{(k^2 + \pi^2)^2}{\Omega k^2}. \quad (3.8e)$$

Note that ϕ_0 involves the, as yet, undetermined σ_{R1} and σ_{I1} . In order to determine σ_{R1} and σ_{I1} we must continue our expansion in δ to the next order. Note that the thermal and flow fields as well as the Rayleigh number (with $S = 0$ so that $\Omega = 1$) correspond to those for convection in a passive porous medium as studied by Palm *et al.* (1972).

At $O(\delta)$ we find that the values of σ_{R1} , σ_{I1} and R_1 are determined via a solvability condition through the modified heat balance and vertical component of Darcy's equation

$$D^2\theta_1 - k^2\theta_1 - \Omega R_0 w_1 = (\sigma_{R1} + i\sigma_{I1} - D) \left(\Omega\theta_0 - \frac{\bar{S}}{C_S} \theta_{B0}\phi_0 \right) + \Omega R_0 w_0 D\theta_{B1} + \Omega R_1 w_0, \tag{3.9a}$$

$$D^2 w_1 - k^2 w_1 - R_0 k^2 \theta_1 = -K_1 D^2 [\phi_{B0} w_0] + k^2 K_1 \phi_{B0} w_0 + k^2 R_1 \theta_0 + K_1 D [w_0 D \phi_{B0}], \tag{3.9b}$$

with boundary conditions $\theta_1(0) = \theta_1(1) = 0$, $w_1(0) = w_1(1) = 0$ and $\phi_1(1) = 0$.

The existence of solutions θ_1 and w_1 requires that the following solvability condition must be satisfied:

$$0 = \frac{(\pi^2 + k^2)^2 K_1}{4 C_S} - (\pi^2 + k^2)^2 \frac{R_1}{R_0} + (\sigma_{R1} + i\sigma_{I1}) \frac{\pi^2 + k^2}{2} \Omega + \frac{\bar{S}}{C_S^2 \Omega} (\pi^2 + k^2)^2 \left[\frac{1}{4} + \frac{\sigma_{R1} + i\sigma_{I1}}{2(\pi^2 + (\sigma_{R1} + i\sigma_{I1})^2)} + \frac{\pi^2(1 + e^{-(\sigma_{R1} + i\sigma_{I1})})}{(\pi^2 + (\sigma_{R1} + i\sigma_{I1})^2)^2} \right]. \tag{3.10}$$

The real and imaginary parts of the characteristic equation (3.10) represent two conditions relating R_1 , σ_{R1} and σ_{I1} . In the following section we seek solutions to equation (3.10) in order to determine the linear stability properties of the mushy-layer system.

4. Stability results

We shall analyse equation (3.10) with the following goals in mind. First, we wish to identify when and if an oscillatory mode ($\sigma_{I1} \neq 0$) can be present. Second, we wish to identify stability boundaries in terms of the Rayleigh number $R = R_0 + \delta R_1$ for both the real and oscillatory modes of instability. Here we distinguish between neutral stability boundaries and boundaries marking the transition between the existence of real modes and the existence of oscillatory modes. Third, we wish to identify the critical value of the Rayleigh number and determine how it varies with the control parameters of the system. Finally, we analyse the structure of oscillatory mode.

4.1. Steady and oscillatory modes

To address the question of the existence of an oscillatory instability we focus first on the neutrally stable case $\sigma_{R1} = 0$. We separate (3.10) into real and imaginary parts and find that the real part determines the Rayleigh number correction R_1 as a function of the frequency σ_{I1} ,

$$\frac{R_1}{R_0} = \frac{1}{4} \frac{K_1}{C_S} + \frac{\bar{S}}{C_S^2 \Omega} \left[\frac{1}{4} + \frac{\pi^2(1 + \cos \sigma_{I1})}{(\pi^2 - \sigma_{I1}^2)^2} \right], \tag{4.1}$$

and the imaginary part determines σ_{I1} as a function of k ,

$$\sigma_{I1} \left\{ 1 + \frac{\bar{S}}{C_S^2 \Omega^2} \frac{\pi^2 + k^2}{\pi^2 - \sigma_{I1}^2} \left[1 - \frac{2\pi^2}{\pi^2 - \sigma_{I1}^2} \frac{\sin \sigma_{I1}}{\sigma_{I1}} \right] \right\} = 0. \quad (4.2)$$

Recall that R_0 is given by equation (3.8e).

We see that $\sigma_{I1} = 0$ is always a solution to equation (4.2). This corresponds to the steady (or real) mode in which case the Rayleigh number (for neutral stability) is given by

$$\begin{aligned} R &= R_0 \left(1 + \delta \frac{R_1}{R_0} \right) + O(\delta^2) \\ &= \Omega^{-1/2} \frac{k^2 + \pi^2}{k} \left[1 + \delta \left(\frac{1}{4} \frac{K_1}{C_S} + \left[\frac{1}{4} + \frac{2}{\pi^2} \right] \frac{\bar{S}}{C_S^2 \Omega} \right) \right] + O(\delta^2). \end{aligned} \quad (4.3)$$

If we focus on the critical wavenumber (the wavenumber which minimizes the value of R), which is given by $k = \pi$, we can compare this result with the results of Amberg & Homsy (1993). In order to make this comparison we note that our Stefan number \bar{S} is assumed to be $O(1/\delta)$ (see (2.10)) while the Stefan number St in Amberg & Homsy (1993) was taken to be $O(1)$ so $\bar{S} = \delta St$. Recalling that $\Omega = 1 + \bar{S}/C_S = 1 + \delta St/C_S$ we find that

$$\begin{aligned} R &= 2\pi + \delta \left[\frac{\pi K_1}{2 C_S} - \frac{\pi St}{C_S} \right] \\ &\quad + \delta^2 \left[\frac{3\pi}{4} \left(\frac{St}{C_S} \right)^2 - \frac{\pi K_1 St}{4 C_S^2} + \left(\frac{\pi}{2} + \frac{4}{\pi} \right) \frac{St}{C_S^2} \right] + O(\delta^2). \end{aligned} \quad (4.4)$$

This expression is correct to $O(\delta)$ and agrees with the results of Amberg & Homsy (see their equations (3.6) and (3.10)). Here we also show those $O(\delta^2)$ terms that appear when we take $\bar{S} = \delta St$ in our approximation because they can be compared with the $O(\delta^2)$ terms involving the Stefan number calculated by Amberg & Homsy (see their equation (3.5b)).

It is also the case that equation (4.2) can have solutions with $\sigma_{I1} \neq 0$. This fact confirms the presence of an oscillatory instability in this system, as was suggested by the weakly nonlinear analysis of the steady mode by Anderson & Worster (1995). A nonzero value of σ_{I1} indicates that the appropriate timescale for the oscillatory instability is $O(\delta)$, i.e. the timescale associated with the mushy-layer thickness and the vertical translation speed of the mushy layer. The significance of this timescale will become more apparent when we analyse the structure of the flow pattern, thermal field and solid fraction. It is also important to note that the possibility of a nonzero frequency σ_{I1} , and hence an oscillatory instability, depends on the single parameter combination $\bar{S}/(C_S^2 \Omega^2)$ (see equation (4.2)). In terms of original, unscaled variables, this is $S/\delta(\mathcal{C} + S)^2$. Unlike the oscillatory instability described by Chen *et al.* (1994), this oscillatory instability is not related to double-diffusive effects or the presence of a statically stable density gradient. The oscillatory instability here is, by the nature of the model, driven solely from the interior of the mushy layer.

Figure 2 shows nonzero solutions σ_{I1} of equation (4.2) as functions of the wavenumber k for different values of the parameter combination $\bar{S}/(C_S^2 \Omega^2)$. For $\bar{S}/(C_S^2 \Omega^2) < 1$ the oscillatory mode exists only for wavenumbers greater than some nonzero value. For $\bar{S}/(C_S^2 \Omega^2) \geq 1$ the oscillatory instability exists for all wavenumbers, including

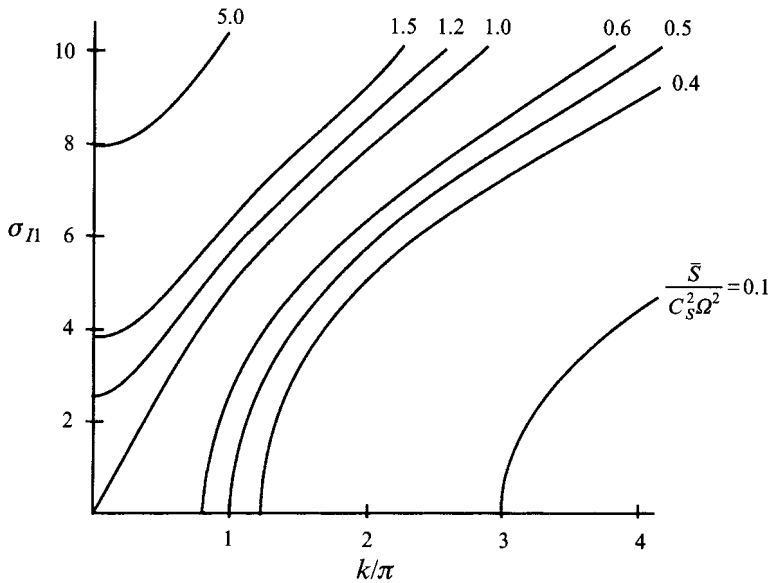


FIGURE 2. $\text{Im}(\sigma)$ vs. wavenumber. The frequency σ_{I1} is shown as a function of the perturbation wavenumber k for different values of the parameter combination $\bar{S}/(C_S^2\Omega^2)$. Nonzero values of σ_{I1} indicate the presence of an oscillatory instability. For $\bar{S}/(C_S^2\Omega^2) < 1$, nonzero σ_{I1} exist only beyond a nonzero wavenumber whose value depends on $\bar{S}/(C_S^2\Omega^2)$. For $\bar{S}/(C_S^2\Omega^2) > 1$ nonzero σ_{I1} exist for all wavenumbers, including zero wavenumber. The first appearance of an oscillatory instability at wavenumber π occurs for $\bar{S}/(C_S^2\Omega^2) = 0.5$.

zero wavenumber. In the weakly nonlinear analysis of Anderson & Worster (1995), the wavenumber corresponding to the steady mode was fixed at its critical value $k = \pi$. They obtained coupled amplitude equations which described small-amplitude convection in the mushy layer and found that, to leading order, the coefficient on the time derivative vanished when $\bar{S}/(C_S^2\Omega^2) = 0.5$ (see their equation (3.16a)). This signalled the presence of an oscillatory instability. If we focus on the wavenumber $k = \pi$ in figure 2 we see that when $\bar{S}/(C_S^2\Omega^2) < 0.5$ the value of σ_{I1} is zero there (i.e. no oscillatory mode is present at the critical wavenumber). However, for $\bar{S}/(C_S^2\Omega^2) > 0.5$, the value of σ_{I1} can be nonzero at $k = \pi$, confirming the presence of an oscillatory mode at the critical wavenumber of the steady mode.

4.2. Stability boundaries

The relation between the steady convective mode and the oscillatory mode can be understood more clearly in plots of the neutral stability curves for the two modes. However, when both real and oscillatory modes are present, it is also necessary to identify the boundary at which the character of the instability changes from real to oscillatory. In fact, we shall demonstrate that often in such cases the boundary associated with neutral stability plays only a secondary role. That is, there may exist growing real modes *outside* the boundaries defined by neutral stability of the real mode (note that these are still linear modes and should be distinguished from subcritical nonlinear instabilities). To characterize this, we focus on the transition between the existence of real modes and the existence of oscillatory modes. Since this transition boundary will not, in general, occur at neutral

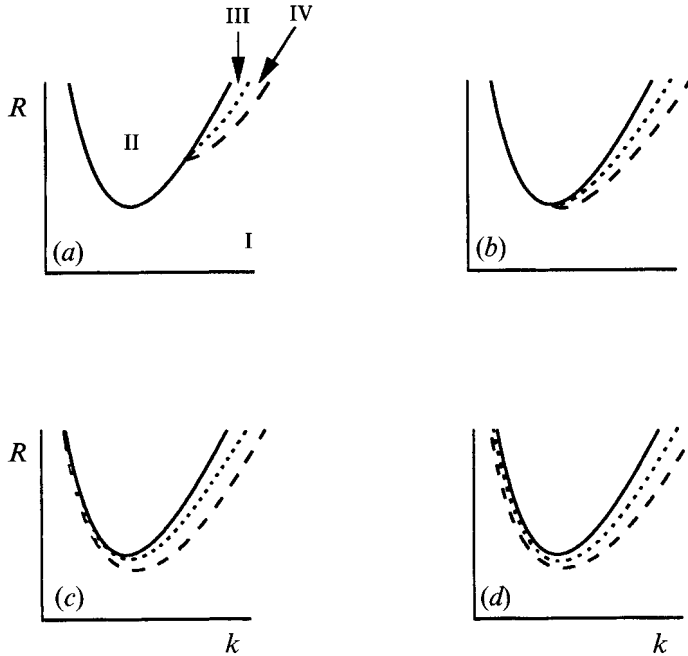


FIGURE 3. The neutral stability curves for the real mode (solid curve), the oscillatory mode (long-dashed curve) and the transition boundary marking the transition between real and imaginary growth rates (short-dashed curve), for representative values (a) $\bar{S}/(C_S^2\Omega^2) < 0.5$, (b) $\bar{S}/(C_S^2\Omega^2) = 0.5$, (c) $\bar{S}/(C_S^2\Omega^2) = 1$ and (d) $\bar{S}/(C_S^2\Omega^2) > 1$. The domains marked in (a) indicate the regions where (I) no growing modes exist, (II) a single growing real mode exists, (III) two growing real modes exist, and (IV) two growing oscillatory modes exist. As the value of $\bar{S}/(C_S^2\Omega^2)$ increases, the point at which the oscillatory branch attaches to the real branch moves in the direction of smaller wavenumbers. In (c) the real and oscillatory branches intersect at $k = 0$ and in (d) they do not intersect.

stability, the full form of equation (3.10), with $\sigma_{R1} \neq 0$, must be analysed. This transition point can be identified mathematically by locating the point in growth rate σ_{R1} vs. k space (for a given R) along the real branch where $d\sigma_{R1}/dk = \infty$ (i.e. a limit point). We have identified this transition, as well as the neutral stability curves for the real and oscillatory modes, numerically and discuss the results below.

Each of the four sketches in figure 3 shows the neutral stability curve for the real mode (solid curve), the neutral stability curve for the oscillatory mode (long-dashed curve) and the transition boundary between the real mode and the oscillatory mode (short-dashed curve) for representative values of $\bar{S}/(C_S^2\Omega^2)$. Figure 3(a) shows the results for a case when $\bar{S}/(C_S^2\Omega^2) < 0.5$ and can be described in terms of the number and type of growing modes for values of Rayleigh number R and wavenumber k within each numbered region. In region I there exist no growing modes. In region II there exists one growing real mode. In region III there exist two growing real modes. In region IV there exist two growing oscillatory modes (one with frequency σ_{I1} and the other with frequency $-\sigma_{I1}$). Note that along the transition boundary between regions III and IV the growth rate σ_{R1} is *nonzero*. Also note that the oscillatory mode attaches to the real mode and thus has an endpoint minimum at which the frequency σ_{I1} is zero.

The other three sketches in figure 3 depict the neutral stability and transition boundaries for (b) $\bar{S}/(C_S^2\Omega^2) = 0.5$, (c) $\bar{S}/(C_S^2\Omega^2) = 1$ and (d) $\bar{S}/(C_S^2\Omega^2) > 1$. In (b) the

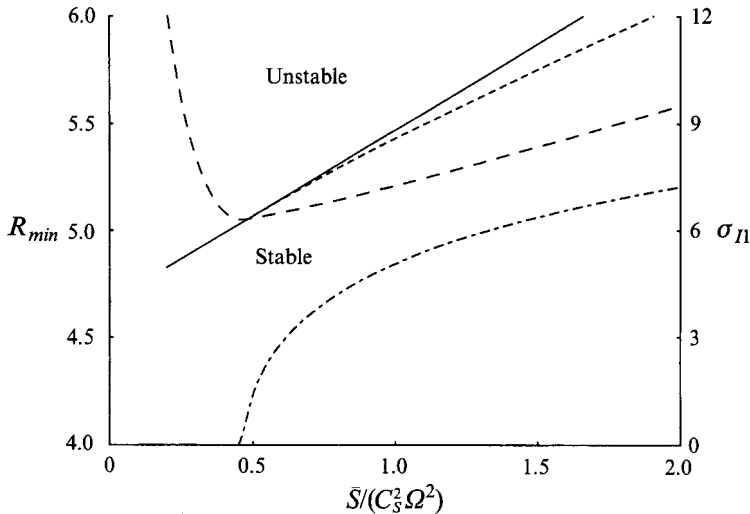


FIGURE 4. Critical Rayleigh number *vs.* $\bar{S}/(C_S^2\Omega^2)$ for $\delta = 0.2$ and $K_1 = \bar{S} = C_S$. The figure indicates the loci of the minimum value of the Rayleigh number corresponding to the real mode (solid curve), the oscillatory mode (long-dashed curve) and the transition boundary (short-dashed curve) which can be associated with the sketches in figure 3. These curves correspond to the left-hand-side axis. Also indicated, and corresponding to the right-hand-side axis, is the frequency σ_{11} (dashed-dotted curve) along the oscillatory branch. There is a transition point near $S/(C_S^2\Omega^2) = 0.5$ below which the minimum of the transition boundary and the minimum of the neutral stability curve for the oscillatory mode coincide and above which the three curves separate.

oscillatory mode attaches to the real mode at the bottom of the neutral curve for the real mode. Note that the minimum of the transition boundary and the minimum of the real mode coincide at $k = \pi$, while the minimum of the oscillatory mode occurs at a wavenumber slightly greater than π . In (c), the oscillatory mode attaches to the real mode at zero wavenumber (infinite Rayleigh number) and therefore exists for all wavenumbers k . In (d), the oscillatory mode again exists for all wavenumbers but now does not intersect the real mode; the oscillatory mode is everywhere less stable than the steady mode.

Figure 4 shows the behaviour of the critical Rayleigh number for the real mode (solid curve), the oscillatory mode (long-dashed curve) and the transition boundary (short-dashed curve) as associated with the results shown in figure 3. Also indicated is the frequency σ_{11} (dashed-dotted curve) along the oscillatory branch (only the positive root is shown). We have noted that the presence of the oscillatory mode depends on the single parameter combination $\bar{S}/(C_S^2\Omega^2)$. However, the Rayleigh number corresponding to neutral stability depends on the parameter combination $\bar{S}/(C_S^2\Omega)$ (see equation (4.1)). Therefore, to illustrate the results, in figure 4 we have chosen to show the case where $\bar{S} = C_S$ so that $\Omega = 2$ and $\bar{S}/(C_S^2\Omega^2) = 1/(4C_S)$. Further, we have fixed $\delta = 0.2$ and have taken $K_1/C_S = 1$. The real mode is the most unstable mode for small values of $\bar{S}/(C_S^2\Omega^2)$ while the oscillatory mode is the most unstable for larger values. The exchange occurs at a value of $\bar{S}/(C_S^2\Omega^2)$ which is slightly less than 0.5. For values of $\bar{S}/(C_S^2\Omega^2)$ to the left of this interchange, the minimum of the transition boundary and the minimum of the oscillatory neutral mode coincide (as can be seen in inset figure 3(a)). For values of $\bar{S}/(C_S^2\Omega^2)$ to the right, the minimum of the transition boundary lies between

that of the oscillatory neutral mode and that of the real neutral mode. For these values, it is important to note that the minimum of the neutral stability curve for the real mode no longer marks the minimum value of R (based on linear theory) for which growing real modes would first be expected to appear. That is, the neutral stability curve for the real mode may no longer provide a good estimate for the onset of a steady mode of instability. The transition boundary now plays this role.

Figures 3 and 4 show that either the real or the oscillatory mode can be the most unstable depending on the value of $\bar{S}/(C_3^2\Omega^2)$. In the interest of identifying ways in which instabilities in the mushy layer can be avoided in practice, we investigate the dependence of the critical Rayleigh number on each of the experimental control parameters S , \mathcal{C} and δ .

4.3. Parametric dependences

Figure 5(a) shows the critical Rayleigh number for the real and oscillatory neutral curves (solid and long-dashed curves, respectively) as well as that for the transition boundary (short-dashed curve, which is in this case nearly coincident with the solid curve) as the Stefan number S varies while the dimensionless mushy-layer thickness δ , compositional ratio \mathcal{C} and linear measure of permeability variations K_1 are fixed ($\delta = 0.1$, $\mathcal{C} = 3$, $K_1 = 3$). Also indicated is the frequency σ_{I1} (dashed-dotted curve) along the oscillatory mode (only the positive root is shown). Note that the ranges for which $\sigma_{I1} = 0$ correspond to endpoint minima. The system becomes more unstable to both real and oscillatory instabilities as the Stefan number increases. The real mode is the most dangerous mode for large and small values of S , while the oscillatory mode is the most dangerous mode for intermediate values. Where the oscillatory mode is the most unstable, the transition boundary marks the smallest value of R at which real modes become unstable (although here it nearly overlaps with that for the neutral real mode itself). Where the real mode is the most unstable, the minimum of the transition boundary coincides with the minimum of the oscillatory mode.

Figure 5(b) shows the minimum Rayleigh numbers for the real and oscillatory modes (solid and long-dashed curves, respectively) and the transition boundary (short-dashed curve) as \mathcal{C} varies while δ , S and K_1 are fixed ($\delta = 0.1$, $S = 5$, $K_1 = 3$). The frequency σ_{I1} (dashed-dotted curve) along the oscillatory mode is also shown. Here the trend in the minimum Rayleigh number for the real and oscillatory modes is qualitatively similar. As discussed by Anderson & Worster (1995), the compositional ratio \mathcal{C} appears in association with a number of parameters. For larger values of \mathcal{C} it appears most strongly in association with the term S/\mathcal{C} and therefore increasing \mathcal{C} has a similar effect to decreasing S . For smaller values of \mathcal{C} , the correction terms associated with the terms K_1/\mathcal{C} and $S/(\mathcal{C}^2\Omega)$ reverse this trend. This trend is limited, however, in that the asymptotic results require $\mathcal{C} \sim O(1/\delta)$.

Figure 5(c) shows the minimum Rayleigh numbers for the real and oscillatory modes (solid and long-dashed curves, respectively) and the transition boundary (short-dashed curve) as δ varies while S , \mathcal{C} and K_1 are fixed ($S = 5$, $\mathcal{C} = 3$, $K_1 = 3$). Again, the frequency σ_{I1} (dashed-dotted curve) along the oscillatory mode is also shown. The minimum of the real mode is, to the order shown, independent of the mushy layer thickness δ (see (4.3) and note $C_S = \delta\mathcal{C}$ and $\bar{S} = \delta S$). Smaller values of δ destabilize the oscillatory mode relative to the real mode.

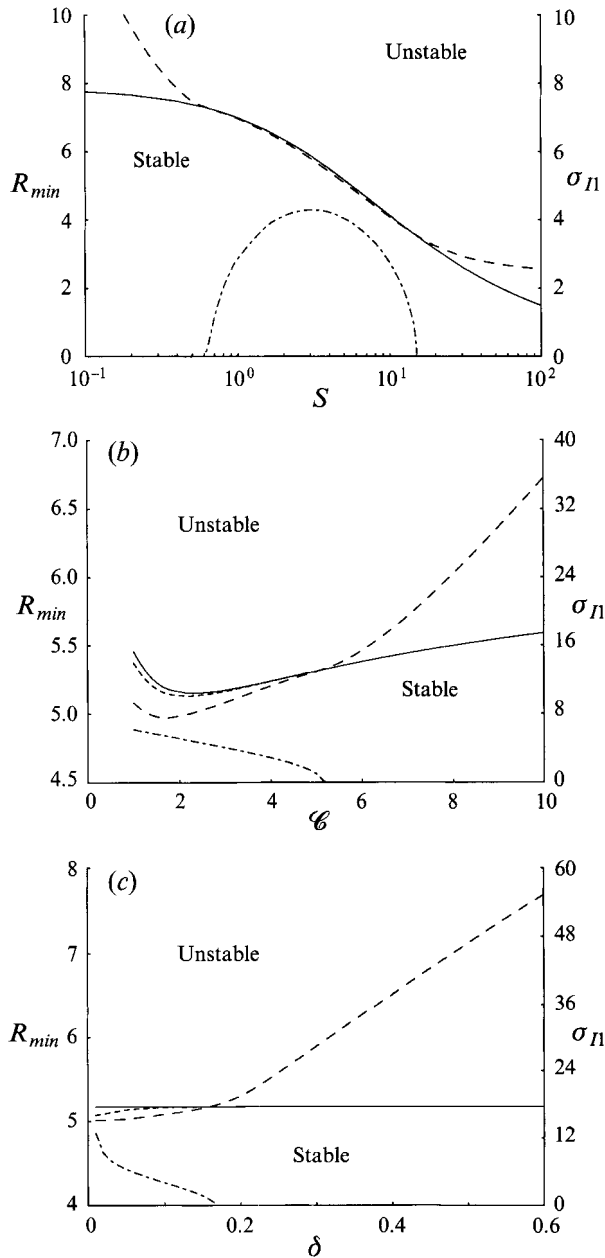


FIGURE 5. The critical Rayleigh numbers as they vary with the dimensionless parameters S , \mathcal{C} and δ , with $K_1 = 3$. The solid curves indicate the critical Rayleigh numbers for the neutrally stable real mode, the long-dashed curves indicate the critical Rayleigh numbers for the neutrally stable oscillatory mode, and the short-dashed curve represents the transition boundary between real and oscillatory modes. The basic-state solution is stable (unstable) below (above) the curves. Also indicated is the frequency σ_{I1} (dashed-dotted curve) along the oscillatory branch. Note that the ranges in which the frequency is zero correspond to those cases where the oscillatory mode has an endpoint minimum and that within these ranges the transition boundary coincides with the critical curve for the oscillatory mode. (a) The variations with S with $\delta = 0.1$ and $\mathcal{C} = 3$. Note that the transition boundary is not resolved on the scale of this figure but lies just below the critical curve for the real mode for $0.6 < S < 15$ approximately and coincides exactly with the critical curve for the oscillatory mode outside this range. (b) The variations with \mathcal{C} with $\delta = 0.1$ and $S = 5$. (c) The variations with δ with $S = 5$ and $\mathcal{C} = 3$. Note that, to the order we have shown, the real mode is independent of the mushy-layer thickness δ .

4.4. Structure of the oscillatory mode

To describe the oscillatory instability further we examine the neutrally stable eigenfunctions representing perturbations to the thermal field, flow field and solid fraction. We combine the basic-state solution and the leading-order perturbations and find

$$\theta = \theta_B + \epsilon[-2 \sin \pi \bar{z} \cos(k\bar{x} + \delta\sigma_{I1}\bar{t})], \quad (4.5a)$$

$$\phi = \phi_B + \epsilon \left[-\frac{2}{\Omega C_S} \frac{\pi(\pi^2 + k^2)}{\pi^2 - \sigma_{I1}^2} \left[\left(\cos \sigma_{I1}(\bar{z} - 1) + \cos \pi \bar{z} \right) \cos(k\bar{x} + \delta\sigma_{I1}\bar{t}) \right. \right. \\ \left. \left. - \left(\sin \sigma_{I1}(\bar{z} - 1) + \frac{\sigma_{I1}}{\pi} \sin \pi \bar{z} \right) \sin(k\bar{x} + \delta\sigma_{I1}\bar{t}) \right] \right], \quad (4.5b)$$

$$w = 0 + \epsilon \left[\frac{2(\pi^2 + k^2)}{\Omega R_0} \sin \pi \bar{z} \cos(k\bar{x} + \delta\sigma_{I1}\bar{t}) \right], \quad (4.5c)$$

$$u = 0 + \epsilon \left[-\frac{2k\pi R_0}{\pi^2 + k^2} \cos \pi \bar{z} \sin(k\bar{x} + \delta\sigma_{I1}\bar{t}) \right], \quad (4.5d)$$

where ϵ is understood to be a small parameter as required by linear theory.

The structure of the solutions (4.5) varies dramatically with the values of the frequency σ_{I1} and wavenumber k (recall that these values are related to physical parameters as indicated in figure 2). First, when $\sigma_{I1} = 0$ these solutions correspond to the well known case of steady convection in the mushy layer. Such solutions are illustrated in figure 6(a) using a laboratory frame of reference where the mushy layer advances upwards at speed V . The perturbations to the solid fraction lead to vertically oriented channels of reduced solid fraction where the flow is upwards. Note that the rising fluid is relatively cold and relatively depleted of solute. Compositional ‘stripes’, which are a record of the mushy-layer history left behind in the solid, result from the variation in solid fraction at the lower boundary of the mushy layer and, in the case of steady convection, are vertically oriented.

When σ_{I1} is nonzero, the solutions (4.5) represent oscillatory states. These may correspond to left or right travelling waves, or any combination thereof, including standing waves. A more detailed analysis taking into account nonlinear effects is required to determine which of these the system selects. For the present purposes, we

FIGURE 6. Neutrally stable eigenfunctions. The mushy layer advances with speed V and the structure of the solutions for three different values of the frequency σ_{I1} are illustrated in a laboratory frame of reference. (a) $\sigma_{I1} = 0$, which correspond to the real mode of convection. Here the solid-fraction channels in the mushy layer and the compositional stripes in the solid are vertically oriented. (b) Typical results for the oscillatory mode of convection when $0 < \sigma_{I1} < 3\pi$. At any instant in time, the convection rolls and thermal fields are, to leading order, vertically oriented. However, as a result of the interaction between the solid-fraction and the thermal and flow fields, the entire pattern translates horizontally as the mushy layer advances. In this case the solid fraction channels have a slope which increases monotonically from $-k/\sigma_{I1}$ at the mush–solid interface to $-3k/\sigma_{I1}$ at the mush–liquid interface. The slope of the compositional stripes in the solid, $-k/\sigma_{I1}$, is determined by the vertical growth velocity of the mushy layer and the horizontal translation speed of the pattern. (c) Typical results for the oscillatory mode of convection when $5\pi < \sigma_{I1} < 7\pi$. The notable difference between this case and that in (b) is that the slope of the solid-fraction channels in the mushy layer now is nonmonotonic. The values of the slope at the bottom and top of the mushy layer are still $-k/\sigma_{I1}$ and $-3k/\sigma_{I1}$, respectively. The slope of the compositional stripes in the solid is again $-k/\sigma_{I1}$.

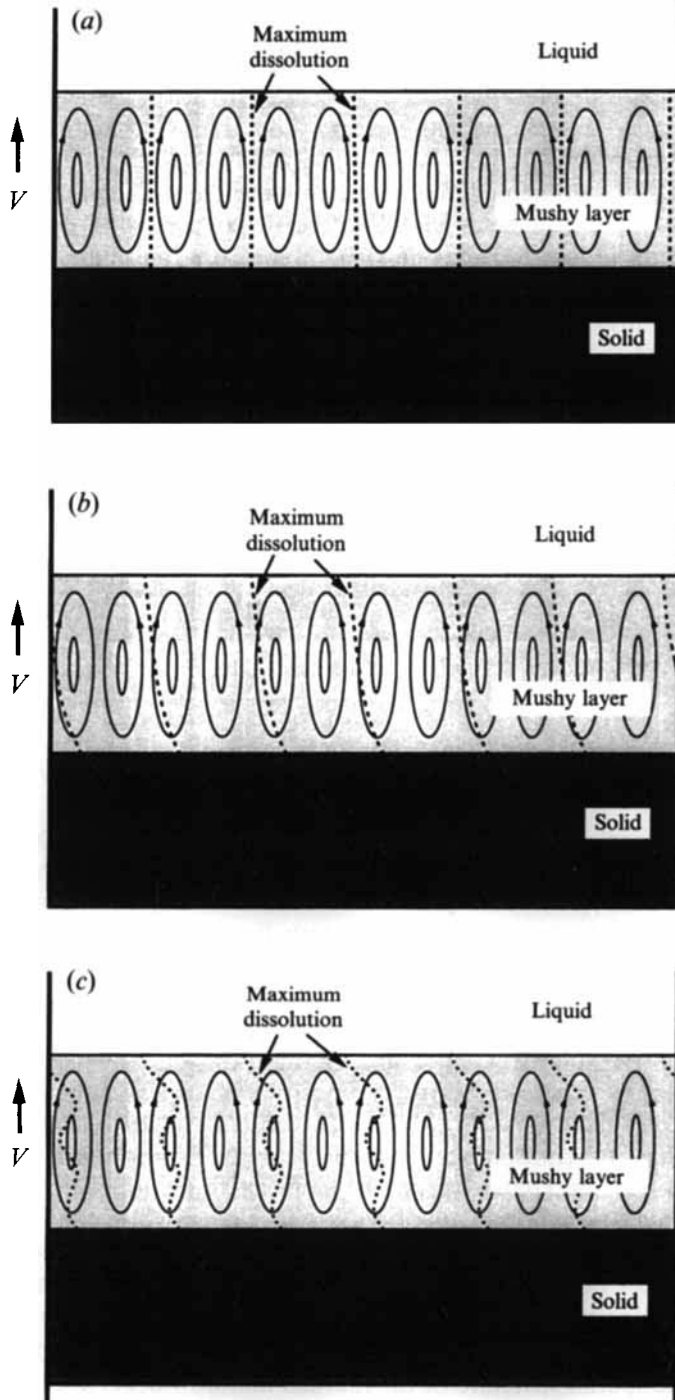


FIGURE 6. For caption see facing page.

shall focus on describing left travelling waves only. The leading-order flow pattern corresponds to vertically oriented convection rolls that translate horizontally as the mushy layer advances. The perturbation to the thermal field translates with the flow and has cold anomalies (solute depleted) associated with the rising fluid and warm anomalies (solute rich) associated with sinking fluid. This horizontal translation can be seen mathematically in equations (4.5a,c,d) by noting that the effect of nonzero σ_{I1} is equivalent to a shift in time of the horizontal coordinate. Therefore, at any instant in time, the thermal and flow fields look like the steady solutions. The leading-order solid-fraction distribution, however, differs both spatially and temporally in relation to its steady-mode counterpart. In addition to translating horizontally at the same rate as the thermal and flow fields, the solid-fraction channels are no longer aligned with the vertical. At the lower boundary of the mushy layer, the slope of the solid-fraction channels is $-k/\sigma_{I1}$ while that at the upper boundary of the mushy layer is $-3k/\sigma_{I1}$. Depending on the value of σ_{I1} the slope may vary monotonically from bottom to top or it may oscillate. Further, the distance Δx between the horizontal coordinate of the channel at $z = \delta$ and that at $z = 0$ also varies. We can quantify these effects as follows:

$$\Delta x = \frac{\sigma_{I1}}{2k}, \quad \text{monotonic slope,} \quad \text{when } 0 \leq \sigma_{I1} < 3\pi, \quad (4.6a)$$

$$\Delta x = \frac{\sigma_{I1}}{2k} - \frac{\pi}{k}, \quad \text{one maximum,} \quad \text{when } 3\pi < \sigma_{I1} < 5\pi, \quad (4.6b)$$

$$\Delta x = \frac{\sigma_{I1}}{2k} - \frac{2\pi}{k}, \quad \text{two maxima,} \quad \text{when } 5\pi < \sigma_{I1} < 7\pi, \quad (4.6c)$$

$$\Delta x = \frac{\sigma_{I1}}{2k} - \frac{3\pi}{k}, \quad \text{three maxima,} \quad \text{when } 7\pi < \sigma_{I1} < 9\pi, \dots \quad (4.6d)$$

A case with $0 < \sigma_{I1} < 3\pi$ is illustrated in figure 6(b). Here the slopes of the solid fraction channels vary monotonically from a value of $-k/\sigma_{I1}$ at the bottom of the mushy layer to $-3k/\sigma_{I1}$ at the top. A case with $5\pi < \sigma_{I1} < 7\pi$ is illustrated in figure 6(c). Note that, in contrast to the pattern for the steady mode, as shown in figure 6(a), the solid-fraction channel away from the upper and lower boundaries of the mushy layer is predominantly within a convective roll, rather than between two convective rolls. There are boundary layers at the top and bottom of the mushy layer where the slopes of the solid-fraction channels attain the values $-3k/\sigma_{I1}$ and $-k/\sigma_{I1}$, respectively. For each of these cases, the compositional stripes left behind in the solid have slope $-k/\sigma_{I1}$, as determined simply by the vertical growth velocity of the mushy layer and the horizontal translation speed of the convection pattern. Therefore, the slope of the solid-fraction channels and the slope of the compositional stripes vary smoothly across the lower boundary of the mushy layer. Note that figure 2 shows that for larger values of $\bar{S}/(C_s^2\Omega^2)$ the value of σ_{I1} gets larger and larger. It is at these larger values of $\bar{S}/(C_s^2\Omega^2)$ that the oscillatory mode is the most dangerous (see figure 4). In principle, then, although figures 4 and 5 show mainly cases where $\sigma_{I1} < 3\pi$, oscillatory states with non-monotonically varying slopes can appear.

The fact that the spatial structure of the thermal and flow fields does not differ from the steady case at leading order is a consequence of the near-eutectic approximation upon which the solutions are based. That is, the leading-order spatial structure of the thermal and flow fields is decoupled from the solid-fraction perturbation so that at any instant in time the convection pattern appears as steady rolls in a passive porous medium of uniform permeability. The leading-order effect of the non-vertically oriented solid-fraction channels on the thermal and flow fields is the

horizontal translation of these fields. Spatial adjustments of thermal and flow fields to the non-vertical solid-fraction channels occur at $O(\delta)$ but are of secondary importance in terms of the driving force behind the oscillatory instability. The fundamental nature of the oscillatory mode is captured by these leading-order results and it is the physical mechanisms involved that we shall elucidate in the next section.

5. Physical mechanisms – a hierarchy of conceptual models

In order to understand the physical mechanisms underlying the oscillatory instability it is useful to identify first those effects which do not play a role. It is clear that the existence of the oscillatory instability does not depend on the presence of nonuniform permeability in the mushy layer since equation (4.2) does not involve K_1 . Therefore the oscillatory instability is not a consequence of reduced flow resistance in the solid-fraction channels. Also, recall that a double-diffusive mechanism can be ruled out since the mushy layer is decoupled from the overlying fluid layer (where stable density gradients may exist) and since the thermal and solutal fields within the mushy layer are directly coupled through the condition of local thermodynamic equilibrium.

Often, oscillatory instabilities can be understood in terms of temporal phase differences between two or more physical quantities present in the system. In the mushy-layer model here, the solid-fraction perturbation is out of phase with the thermal and flow fields when $\sigma_{I1} \neq 0$ (as can be seen mathematically from equations (4.5)) and, as demonstrated in the previous section, the result is oscillatory motion.

With these ideas in mind, we formulate a series of simple conceptual models that illustrate how the ideas of convection in mushy layers have developed in recent years and help to reveal the physical mechanisms responsible for the oscillatory instability.

Consider first the system of ordinary differential equations

$$\dot{W} = (R - 1)W, \quad \dot{\phi} = -\mathcal{C}^{-1}W, \tag{5.1a,b}$$

where W represents a (vertical) velocity, ϕ represents the perturbation to the solid fraction and the dot indicates a derivative with respect to time. Equation (5.1a) represents conceptually convection in a passive porous layer which is triggered when a Rayleigh number R exceeds a critical value, here set equal to unity. The convection causes transport of solute, which alters the solid fraction through equation (5.1b). The solid fraction decreases when W is positive (upwards). This is the fundamental mechanism responsible for the formation of chimneys (cf. Fowler 1985). Within the constraints of this conceptual model, in which the flow is decoupled from the solid fraction, no oscillations are possible.

An important mechanism within mushy layers is the release of latent heat as solid grows. This effect is incorporated in the system of equations

$$\dot{W} = (R - 1)W - S\dot{\phi}, \quad \dot{\phi} = -\mathcal{C}^{-1}W. \tag{5.2a,b}$$

Recall that higher temperatures in the mushy layer correspond to more solute-laden interstitial fluid and hence to negative buoyancy. The release of latent heat, measured by the Stefan number S , thus serves to retard the growth of the vertical velocity, as illustrated by equation (5.2a). The equations are now seemingly coupled but they can be combined to give

$$\dot{W} = (R - 1 + S/\mathcal{C})W. \tag{5.3}$$

Thus the convective problem is again decoupled (cf. Emms & Fowler 1994). It can

be seen that the effect of increasing the Stefan number is to render the system more unstable to convection (cf. Worster 1992*b*). The system (5.2) encapsulates the essential physical mechanisms that have been recognized to date, and no mechanism there is capable of producing oscillations.

Equation (5.2*b*) attempts to mimic the solute-conservation equation, which states that the rate of change of the bulk composition is proportional to the rate of transport of solute. The term on the left-hand side of equation (5.2*b*) comes from the rate of change of solute within the solid fraction of the mushy layer. An additional term is required to represent the overall solidification as the whole system is cooled, which alters the solute within the liquid fraction of the mushy layer. A better model of the perturbed solute-conservation equation is given by

$$\dot{\phi} + V\phi = -\mathcal{E}^{-1}W. \quad (5.4)$$

The additional term associated with the solidification rate V causes a decay of the solid fraction to its equilibrium value in the absence of flow ($W = 0$). It is this decay that finally allows the model to predict oscillations by introducing a phase lag between the dissolution caused by the flow and the solidification caused by overall cooling. Equations (5.2*a*) and (5.4) can be combined to give

$$\dot{W} = (R - 1 + S/\mathcal{E})W + SV\phi, \quad \dot{\phi} = -\mathcal{E}^{-1}W - V\phi. \quad (5.5a,b)$$

These equations now encapsulate the essential balances in the perturbation equations (3.2). The fact that the off-diagonal terms on the right-hand side of equations (5.5) are of opposite sign indicates that oscillations are possible. It is straightforward to show that the coupled system (5.5) has eigensolutions proportional to $e^{\sigma t}$ with

$$2\sigma = (R - 1 + S/\mathcal{E} - V) \pm [(R - 1 + S/\mathcal{E} + V)^2 - 4VS/\mathcal{E}]^{1/2}. \quad (5.6)$$

The location of these growth rates in the complex plane is shown in figure 7. It shows the neutral curves for real and oscillatory modes as well as the transition boundary between real and oscillatory modes. This figure has the same topology as the growth rates for the full linear system analysed in §3. Specifically, we note that the following comparison between figure 7 and figure 3(*a*) applies. In figure 7, above the real neutral curve there is one growing real mode (analogous to region II in figure 3*a*). Between the real neutral curve and the transition boundary there are two growing real modes (analogous to region III in figure 3*a*). Between the transition boundary and the oscillatory neutral curve there are two growing oscillatory modes (analogous to region IV in figure 3*a*). Between the oscillatory neutral curve and the real neutral curve there are no growing modes of either type (analogous to region I in figure 3*a*). The conceptual model thus seems to capture the essential mechanisms underlying the oscillatory instability newly discovered in this paper.

6. Conclusion

We have performed a linear stability analysis of convection in a mushy layer during the solidification of binary alloys. Our analysis is based on a simple model of the mushy layer given by Amberg & Homsy (1993) in which the dynamics of the mushy layer are decoupled from the dynamics of the overlying fluid layer.

We have identified an oscillatory instability, which, to our knowledge, has not been reported previously. In particular, the oscillatory instability found here is distinct from that in Chen *et al.* (1994), which arose due to double-diffusive convection

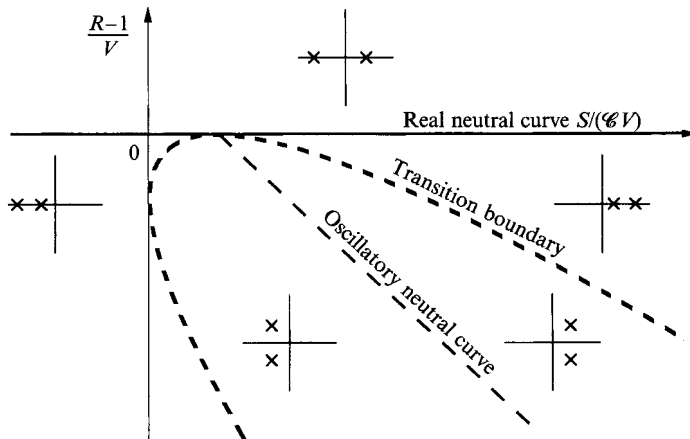


FIGURE 7. The character of the growth rates predicted by the conceptual model. The insets show the locations of the two normal-mode growth rates in the complex plane. The system is unstable when at least one of the roots has a positive real part. The diagram shows the neutral curves for real and oscillatory modes and the transition boundary where two real modes combine to form a complex-conjugate pair.

associated with the presence of an overlying liquid layer in which stabilizing thermal buoyancy was present. In the model we analyse here, there is no overlying liquid layer and double-diffusive effects are not present in the mushy layer owing to the strong coupling between the thermal and solute fields as imposed by the condition of thermodynamic equilibrium. The oscillatory mode here is driven by a mechanism internal to the mushy layer. Through the use of a series of illustrative models, we have shown that this mechanism involves an intricate coupling between convection, heat transfer and solidification. More specifically, we find that the oscillatory instability can be identified with a phase difference between the thermal and flow fields and the solid fraction which results from the interaction between cooling driving the solid fraction perturbation towards an equilibrium value and the tendency of fluid motion to amplify the solid-fraction perturbation.

We have analysed the behaviour of the oscillatory instability as well as the real mode of instability in terms of the critical Rayleigh number at which each first appears. The results show that either mode can be the most unstable mode. We have shown that in addition to identifying the neutral stability boundaries for each mode, it is also necessary to identify the boundary marking the transition from oscillatory to real instability. This transition boundary plays a particularly important role when the oscillatory mode is the most unstable mode, since, in those cases, the transition boundary corresponds to smaller values of the Rayleigh number than the neutral stability curve for the real mode. In such cases, the neutral stability curve for the real mode may no longer be a good estimate for the onset of the real mode of instability.

The results of figures 4 and 5 suggest that small values of δ and \mathcal{C} promote oscillatory instability more than larger values. More generally, an $O(1)$ value for the parameter group $S/\delta(S + \mathcal{C})^2$ is required for oscillations. In an experiment, it is possible to vary the base-plate temperature (and hence the Stefan number S), the initial composition (and hence \mathcal{C}) and the far-field, or furnace, temperature (and hence δ). Note that increasing the pulling speed V will not affect $\delta = dV/\kappa$ since the mushy-layer depth d in an experiment will vary in direct proportion to $1/V$. In an industrial setting, the temperature at the base of the mushy layer is typically the

eutectic temperature, since castings are solidified completely, so that once the material for a turbine blade, for example, is chosen, both S and \mathcal{C} are fixed. Therefore, for a given material the only control parameter is $\delta \sim 1/\theta_\infty$ (i.e. the furnace temperature). Our results indicate that small values of δ , or large furnace temperatures, favour the oscillatory mode. Materials that allow smaller values of \mathcal{C} would be more likely to exhibit the oscillatory instability than those which have large values of \mathcal{C} . Note that aqueous solutions of ammonium chloride that can conveniently be made in the laboratory (i.e. at room temperature) typically have large values of \mathcal{C} (≈ 20) and hence may not be a good candidate.

We have made preliminary calculations using a model of a mushy layer that replaces the condition of zero velocity at the upper boundary of the mushy layer with a condition of zero pressure (which allows inflow and outflow through the upper surface) to test the robustness of the present oscillatory instability. Specifically, we calculated the leading-order coefficient that would appear on the time derivative of amplitude equations describing small-amplitude convection. Where Anderson & Worster (1995) found this value to be $\Omega - 2\bar{S}/(C_S^2\Omega)$ (zero-velocity condition) we obtain $\Omega - 2.46\bar{S}/(C_S^2\Omega)$ (zero-pressure condition). While we stress that we have not carried out a full investigation of the effect of a zero-pressure condition for this model, this result indicates that an oscillatory instability is still present though at modified values of the parameters.

Also, preliminary calculations for the two-layer mushy-layer model of Worster (1992*b*) with the buoyancy ratio (ratio of stabilizing thermal buoyancy to destabilizing solutal buoyancy) in the liquid layer set to zero indicate topology in the real value of the linear growth rate consistent with the presence of an oscillatory instability. Further quantification of this remains to be done.

The results of this paper seem to indicate that, although an oscillatory mode may be the most critical in some circumstances, it will give way to a steady mode of convection at larger values of the Rayleigh number. It also seems likely that channel formation due to nonlinear variations in the local permeability of mushy layers will tend to lock the flow into steady patterns. Therefore, in practice, oscillatory modes of convection may be confined to situations close to marginal conditions. Such may nevertheless be the case industrially if controls are put on a casting process that weaken convection but fail to eliminate it completely or in geological situations in which the large viscosity of magmas may keep convection weak within cumulate layers, for example. In these cases the most telling observation is likely to be striations of texture and bulk composition of the solidified material (figure 6) tilted with respect to the direction of solidification, so that a vertical sample through the solid, say, would contain layers alternating between relatively high and relatively low compositions.

Perhaps the most important consequence of the present study is not the identification of oscillatory modes of convection *per se* but that this phenomenon has highlighted an important and hitherto unsuspected interaction between convection and solidification that can occur within mushy layers.

This work was supported by grants from the National Aeronautics and Space Administration through the Microgravity Science and Applications Division and from the Natural Environment Research Council. The authors would like to thank B. J. Spencer and J. R. Lister for helpful discussions and J. S. Wettlaufer for helpful comments on an earlier draft of this paper.

REFERENCES

- AMBERG, G. & HOMSY, G. M. 1993 Nonlinear analysis of buoyant convection in binary solidification with application to channel formation. *J. Fluid Mech.* **252**, 79–98.
- ANDERSON, D. & WORSTER, M. G. 1995 Weakly-nonlinear analysis of convection in a mushy layer during the solidification of binary alloys. *J. Fluid Mech.* **302**, 307–331.
- BENNON, W. D. & INCROPERA, F. P. 1987 A continuum model for momentum, heat and species transport in binary solid–liquid phase change systems—I. Model formulation. *Intl J. Heat Mass Transfer* **30**, 2161–2170.
- CHEN, C. F. & CHEN, F. 1991 Experimental study of directional solidification of aqueous ammonium chloride solution. *J. Fluid Mech.* **227**, 567–586.
- CHEN, F., LU, J. W. & YANG, T. L. 1994 Convective instability in ammonium chloride solution directionally solidified from below. *J. Fluid Mech.* **276**, 163–187.
- COPLEY, S. M., GIAMEI, A. F., JOHNSON, S. M. & HORNBECKER, M. F. 1970 The origin of freckles in unidirectionally solidified castings. *Metall. Trans.* **1**, 2193–2204.
- EMMS, P. W. & FOWLER, A. C. 1994 Compositional convection in the solidification of binary alloys. *J. Fluid Mech.* **262**, 111–139.
- FOWLER, A. C. 1985 The formation of freckles in binary alloys. *IMA J. Appl. Maths* **35**, 159–174.
- HILLS, R. N., LOPER, D. E. & ROBERTS, P. H. 1983 A thermodynamically consistent model of a mushy zone. *Q. J. Mech. Appl. Maths* **36**, 505–539.
- KURZ, W. & FISHER, D. J. 1989 *Fundamentals of Solidification*. Trans Tech.
- PALM, E., WEBER, J. E. & KVERNVOLD, O. 1972 On steady convection in a porous medium. *J. Fluid Mech.* **54**, 153–161.
- SAMPLE, A. K. & HELLAWELL, A. 1984 The mechanisms of formation and prevention of channel segregation during alloy solidification. *Metall. Trans.* **15A**, 2163–2173.
- SARAZIN, J. R. & HELLAWELL, A. 1988 Channel formation in Pb–Sn, Pb–Sb, and Pb–Sn–Sb alloy ingots and comparison with the system $\text{NH}_4\text{Cl}-\text{H}_2\text{O}$. *Metall. Trans.* **19A**, 1861–1871.
- TAIT, S., JAHRLING, K. & JAUPART, C. 1992 The planform of compositional convection and chimney formation in a mushy layer. *Nature* **359**, 406–408.
- TAIT, S. & JAUPART, C. 1992 Compositional convection in a reactive crystalline mush and melt differentiation. *J. Geophys. Res.* **97(B5)**, 6735–6756.
- VOLLER, V. R. & BRENT, A. D. 1989 The modelling of heat, mass and solute transport in solidification systems. *Intl J. Heat Mass Transfer* **32**, 1719–1731.
- WORSTER, M. G. 1986 Solidification of an alloy from a cooled boundary. *J. Fluid Mech.* **167**, 481–501.
- WORSTER, M. G. 1991 Natural convection in a mushy layer. *J. Fluid Mech.* **224**, 335–359.
- WORSTER, M. G. 1992a The dynamics of mushy layers. In *Interactive Dynamics of Convection and Solidification* (ed. S. H. Davis, H. E. Huppert, U. Müller & M. G. Worster), pp. 113–138. Kluwer.
- WORSTER, M. G. 1992b Instabilities of the liquid and mushy regions during solidification of alloys. *J. Fluid Mech.* **237**, 649–669.